Support information

15.34% Efficiency All-Small-Molecule Organic Solar Cells with Improved Fill Factor Enabled by a Fullerene Additive

Dingqin Hu[a], Qianguang Yang[a], Haiyan Chen[a], Friso Wobben[b], Vincent M. Le Corre[b], Ranbir Singh[c], Tao Liu[d], Ruijie Ma[d], Hua Tang[a], L. Jan Anton Koster[b], Tainan Duan[a], He Yan[d], Zhipeng Kan [a]* Zeyun Xiao [a]*, and Shirong Lu [a]*

[a] Chongqing Institute of Green and Intelligent Technology, Chongqing School, University of Chinese Academy of Sciences (UCAS Chongqing), Chinese Academy of Sciences, Chongqing, 400714, China

[b] Zernike Institute for Advanced Materials, University of Groningen, Nijenborgh 4, NL-9747AG Groningen, The Netherlands

[c] Department of Energy & Materials Engineering, Dongguk University, Seoul, 100-715, Republic of Korea

[d] Department of Chemistry and Hong Kong Branch of Chinese National Engineering Research Center for Tissue Restoration & Reconstruction, Hong Kong University of Science and Technology (HKUST), Clear Water Bay, Kowloon, Hong Kong, China

E-mail: kanzhipeng@cigit.ac.cn; xiao.z@cigit.ac.cn; lushirong@cigit.ac.cn;

Experimental Section

1. Materials

All reagents and solvents, unless otherwise specified, were purchased from Energy Chemical, Tansoole, Suna Tech, Aldrich and JiangSu GE-Chem Biotech., Ltd. and were used without further purification. $PC_{71}BM$, $PC_{60}BM$, $PC_{71}BM$-C and Y6 were purchased from Solarmer Energy Inc. Phen-NaDPO was purchased from 1 materials. BTR-Cl was synthetized following previous reports.

2. Thin film Characterizations

i. Ultraviolet−visible light (**UV-vis**) absorbance spectra were recorded on a Perkin Eimer Lambda 365 spectrophotometer. **Contact angle** was measured by DSA-100 (KRUSS Germany).

ii. Topographic images of the films were obtained from a Bruker atomic force microscopy (**AFM**) with the type of dimension edge with Scan AsystTM in the tapping mode using an etched silicon cantilever at a nominal load of ~2nN, and the scanning rate for a 2 μm×2 μm image size was 1.5 Hz.

iii. Transmission electron microscope (**TEM**) studies were conducted with a Talos F200S electron microscopy to investigate the phase distribution of the active layer.

iv. Ellipsometric (EM) measurements and data analysis: The films were prepared on optical glasses following the active layer conditions and tested with the M-2000 Ellipsometer. The measured data were fitted with the software CompleteEASE with two steps: 1) Cauchy model was applied to fit the transparent region, and it was set starting from 1000 nm to longer wavelength; 2) then Bspline model was applied to parameterize the layer and expanded the fitting range to the whole spectra. The fitting quality was evaluated by the MSE values, and MSE values of 13.76 and 17.92 were obtained for the films w/o and with PC71BM, respectively. The experimental data were well fitted by the models applied as shown in Figure S3 a, and b (black dots).

v. Grazing-Incidence wide-angle X-ray scattering (**GIWAXS**) measurements were carried out at 5A beamline of the Pohang Light Source II (PLS-II) in South Korea. The GIWAX images were recorded at 0.13 incidence angle with X-rays of 11.57 keV (λ=1.0716Å) and MAR345 image plate detector.

vi. GISAXS measurement were carried out with a Xeuss 2.0 SAXS laboratory beamline using a Cu X-ray source (8.05 keV, 1.54 Å) and a Pilatus3R 300K detector. The incidence angle is 0.2°.

3. Device Fabrication and characterizations

The device structures were ITO/PEDOT:PSS/Active layer/Phen-NaDPO/Ag. ITO coated glass substrates were cleaned with detergent water, deionized water, acetone and isopropyl alcohol in an ultrasonic bath sequentially for 30 min, and further treated with UV exposure for 30 min in a UV-ozone chamber. A thin layer (ca. 30 nm) of PEDOT:PSS (Bayer Baytron 4083) was first spin-coated on the substrates with 4000 rpm and baked at 120 °C for 10 min under ambient conditions. The substrates were then transferred into a nitrogen-filled glove box. The optimized concentration was 17 mg/ml chloroform solution with D:A ratio of 1.8:1 (w/w). After spin coating, the blend films were treated with chloroform solvent for 30 s and annealed at 120 °C for 5 mins. The active layer thickness was around 120 nm. Then Phen-NaDPO as the electron transporting layer was spin-coated on the active layer by 2000 rpm from isopropyl alcohol solution. Finally, the substrates were transferred to a thermal evaporator, and top electrode was evaporated at a pressure of 2×10^{-5} Pa.

The external quantum efficiency (*EQE*) was performed using certified IPCE equipment (Zolix Instruments, Inc, Solar Cell Scan 100). The *J–V* curves were measured under AM 1.5 G (100 mW cm^{-2}) (Enli Technology Co., Ltd. SS-X50R).

The *J–V* measurement signals were recorded by a Keithley 2400 source-measure unit. Device area of each cell was 0.08636 cm^2.

4. SCLC Mobility Measurements

The carrier mobility (hole and electron mobility) of photoactive layer was determined by fitting the dark current of hole/electron-only diodes to the space-charge-limited current (SCLC) model. Hole-only diode configuration: Glass/ITO/PEDOT:PSS/active layer/MoO_3/Ag; Electron-only diode configuration: Glass/ITO/ZnO/Phen-NaDPO/active layer/Phen-NaDPO/Ag. V_{bi}=0 was used for both fittings. The active layer thickness was determined by a Tencor surface profilometer. The electric-field dependent SCLC mobility was estimated using the following equation:

$$J(V) = \frac{9}{8}\varepsilon_0\varepsilon_r\mu_0 exp\left(0.89\beta\sqrt{\frac{V - V_{bi}}{L}}\right)\frac{(V - V_{bi})^2}{L^3}$$

5. 1D drift diffusion simulations

All the simulations are based on a home-built 1-dimensional drift-diffusion device model.[1] Employing drift-diffusion simulations permits the calculation of current-voltage characteristics, by solving the Poisson and continuity equations, see below. In this simulation the charge carriers can move by either the effect of the electric-field—drift—or due to the gradient of the charge carrier concentrations—diffusion.

-Poisson equation:

$$\frac{\partial^2\Psi(x)}{\partial x^2} = \frac{q}{\epsilon}(n(x) - p(x))$$

-Continuity equations:

$$J_n(x) = -q\mu_n n(x)\frac{\partial\Psi(x)}{\partial x} + qD_n\frac{\partial n(x)}{\partial x}$$

$$J_p(x) = -q\mu_p p(x)\frac{\partial\Psi(x)}{\partial x} - qD_p\frac{\partial p(x)}{\partial x}$$

$$\frac{\partial J_n(x)}{\partial x} = -q(G(x) - R(x))$$

$$\frac{\partial J_p(x)}{\partial x} = q(G(x) - R(x))$$

-Bimolecular recombination:

$$R = k_{BR}\left(np - n_i^2\right)$$

where x denotes the position in the device, Ψ the potential, n (p) the electron (hole) charge carrier density, Jn(p) the electron (hole) current, q the electronic charge, ε the dielectric constant, n_i the intrinsic carrier concentration, G and R the generation and recombination rates.

In this simulation, the active layer of the BHJ solar cell is modeled using an effective medium approximation that considers the BHJ as a one-phase semiconductor. The highest occupied molecular orbital (HOMO) of the effective semiconductor is taken as the HOMO value of the donor BTR-Cl, and the lowest unoccupied molecular orbital (LUMO) of the effective semiconductor is taken as the LUMO value of the acceptor Y6 for the binary device. For the Ternary device we chose the HOMO to be the HOMO of the donor BTR-Cl and the lower LUMO of the two acceptors, here, $PC_{71}BM$. The fits were performed by simultaneously minimizing the difference between simulated and experimental data for several light intensities.

Trapping was also considered at first as a potential recombination pathway, however, the best fits were always obtained without trapping which suggests that the control and optimized device are both limited by bimolecular recombination and not trapping.

Figure S1. Independent certification by the National Institute of Metrology of optimized devices confirming a stability *PCE* of 14.7%.

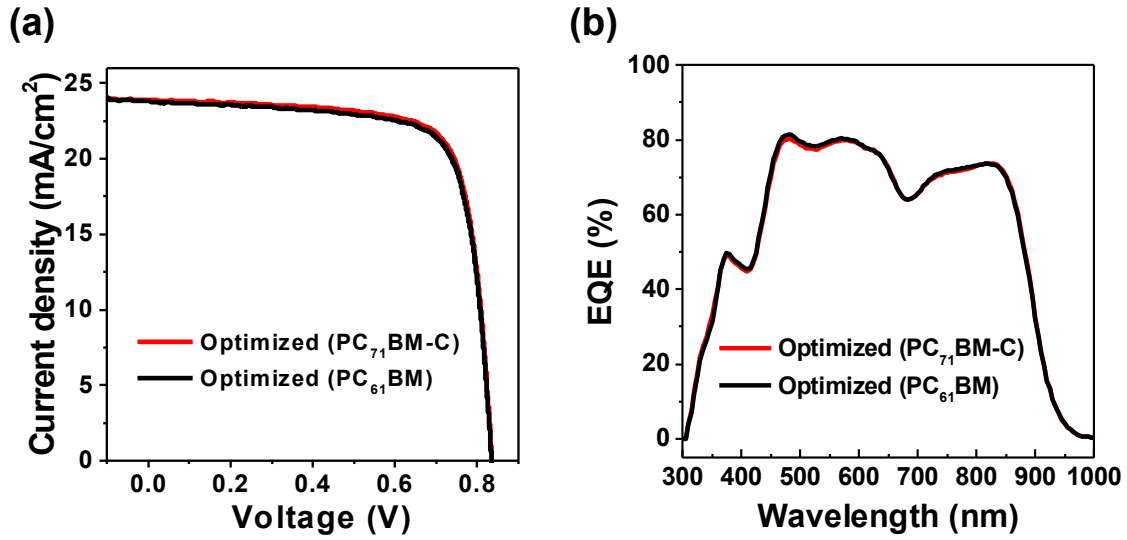

Figure S2. Current density (*J-V*) and curves of control and optimized devices with $PC_{71}BM$-C and $PC_{61}BM$.

Table S1. Summary of photovoltaic performance in optimized devices with adding $PC_{61}BM$ and $PC_{71}BM$-C.

Device Condition	V_{oc} (mV)	J_{sc} (mA/cm²)	*FF* (%)	[a] *PCE*(%)	[b] J_{sc} (mA/cm²)
Optimized C_{61}	835.1(835±0.55)	23.95(23.88±0.07)	75.57(75.28±0.35)	15.12(15.01±0.12)	23.88
Optimized C_{71}-C	835.9(835.5±0.81)	23.89(23.85±0.05)	76.11(75.67±0.44)	15.20(15.08±0.11)	23.81

a) Statistical data obtained from at least 10 devices. b) The Jsc calculated from external quantum efficiency (EQE) curve.

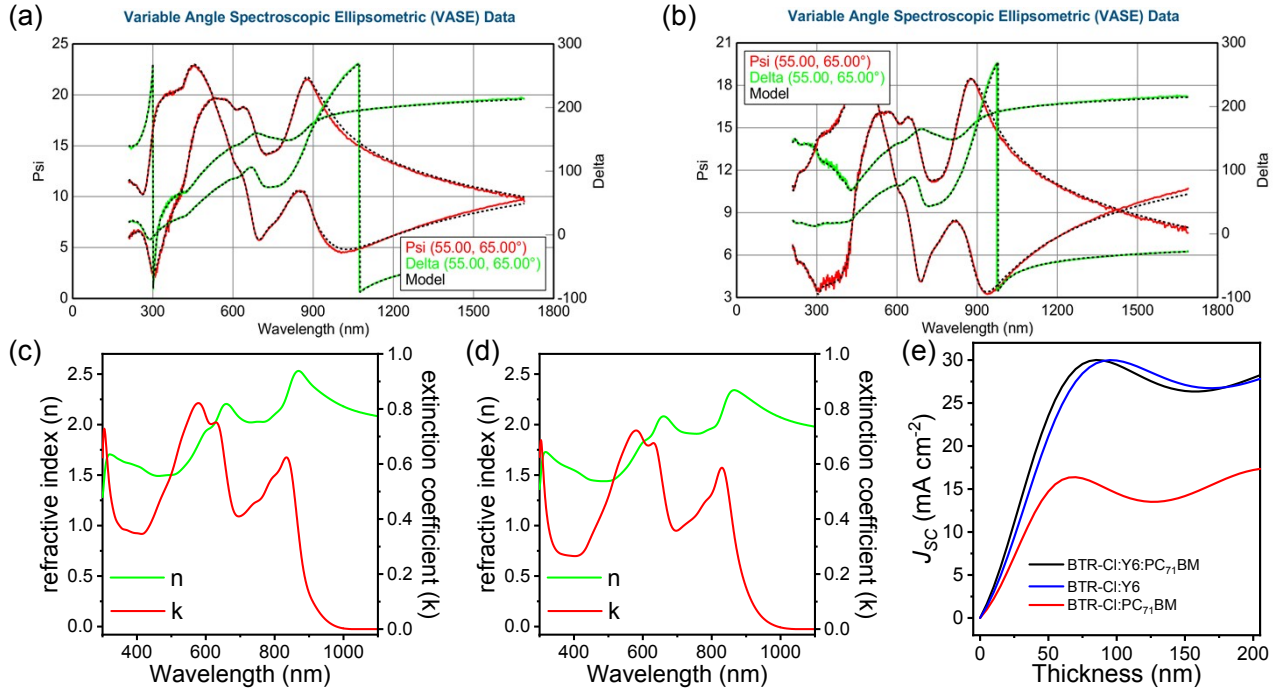

Figure S3. Data fitting to the ellipsometer measurements (a) film with $PC_{71}BM$ and (b) film w/o $PC_{71}BM$; n and k values for (c) film with $PC_{71}BM$ and (d) film w/o $PC_{71}BM$; (e) simulated current density as a function of active layer thickness.

Table S2. Summary of photovoltaic performance in optimized devices with different adding of $PC_{71}BM$.

BTRCl:$PC_{71}BM$:Y6	V_{oc} (mV)	J_{sc} (mA/cm^2)	*FF* (%)	[a] *AvgPCE* (%)	*Max PCE* (%)	[b] J_{sc} (mA/cm^2)
1:1:0	953.2±0.18	10.49±0.28	54.78±0.96	5.47±0.19	5.86	10.08
1.8:0:1	833.3±0.38	23.76±0.05	69.15±0.54	13.69±0.12	13.81	23.71
1.8:1:0.05	834.9±0.21	23.66±0.09	74.76±0.58	14.77±0.18	15.03	23.74
1.8:1:0.1	837.1±0.61	23.71±0.04	76.26±0.62	15.14±0.15	15.34	23.65
1.8:1:0.15	838.5±0.48	23.37±0.07	74.6±0.73	14.62±0.18	14.89	23.33
1.8:1:0.2	839.0±0.22	23.09±0.09	74.56±0.50	14.45±0.15	14.65	23.02
1.8:1:0.3	839.7±0.77	22.64±0.11	73.36±0.58	13.94±0.18	14.18	23.56

a) Statistical data obtained from at least 15 devices. b) The *J*sc calculated from external quantum efficiency (*EQE*) curve.

Table S3. Electron mobility (μ_e), hole mobility (μ_h) and μ_h/μ_e of BTR-Cl:$PC_{71}BM$, control and optimized devices.

Device condition	μ_e ($\times 10^{-4}$ cm^2 V^{-1} s^{-1})	μ_h ($\times 10^{-4}$ cm^2 V^{-1} s^{-1})	μ_h/μ_e
BTR-Cl:$PC_{71}BM$	33.1 (31.2 ± 1.8)	47.2 (45.8 ± 1.4)	1.43 (1.47 ± 0.09)
Control	9.13 (9.01 ± 0.1)	9.97 (9.84 ± 0.11)	1.09 (1.11 ± 0.02)
Optimized	9.32 (9.19 ± 0.1)	9.78 (9.62 ± 0.13)	1.05 (1.07 ± 0.02)

The mobility values were averaged from 10 devices.

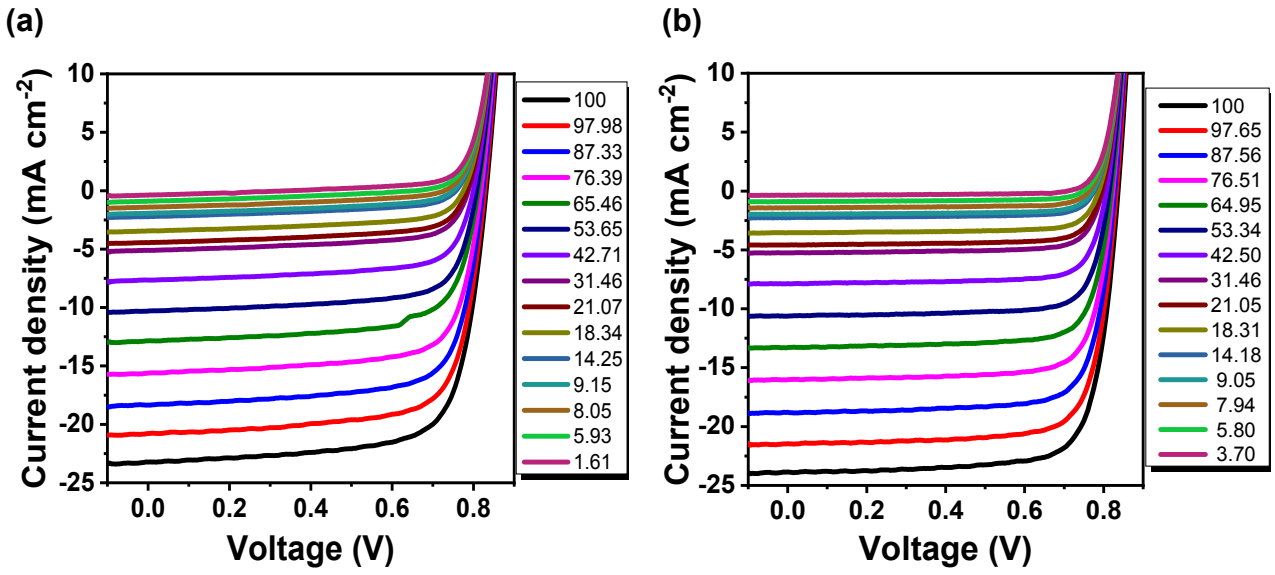

Figure S4. Current density (*J-V*) curves of control and optimized devices are used for simulation with different light intensity.

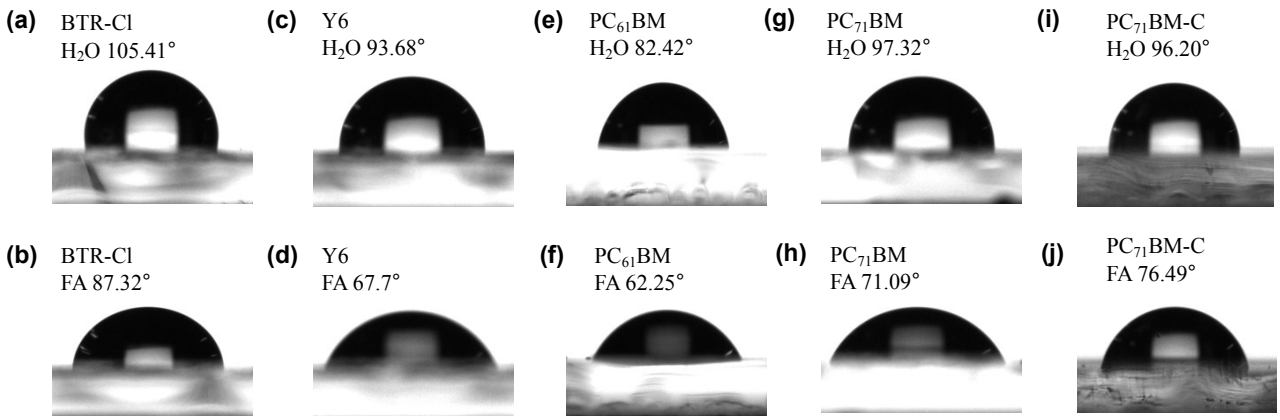

Figure S5. Contact angle with deionized water and formamid of BTR-Cl, Y6, $PC_{61}BM$, $PC_{71}BM$ and $PC_{71}BM$-C films.

Table S4. Contact angle with deionized water, formamid and surface free energy of $PC_{71}BM$, Y6, BTR-Cl and $PC_{61}BM$ films

Film	Contact angle		Contact angle		Surface free energy (mN/m)
	H_2O (°)	**Average (°)**	**FA (°)**	**Average (°)**	
	105.41		87.02		
BTR-Cl	105.98	105.51	87.28	87.21	18.3
	105.15		87.32		
	93.68		67.7		
Y6	93.33	93.13	66.79	66.98	33.49
	92.39		66.46		
	82.00		62.48		
$PC_{61}BM$	82.42	81.87	62.25	61.97	32.10
	81.20		61.18		
	97.32		71.64		
$PC_{71}BM$	97.02	97.25	71.09	71.58	31.04
	97.41		72.01		
$PC_{71}BM$-C	96.20	96.34	75.15	76.29	

96.31	76.49	24.51
96.51	77.23	

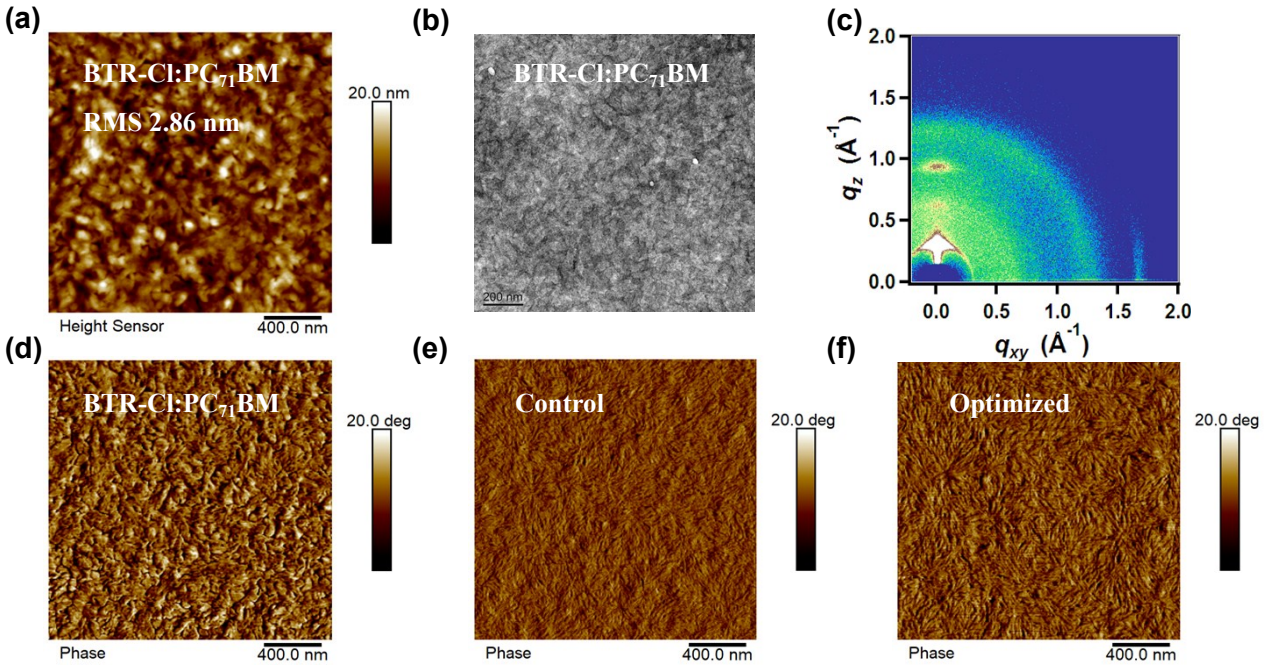

Figure S6. (a) AFM images (2×2 μm), (b) TEM images and (c) 2D GIWAXS patterns of BTR-Cl:$PC_{71}BM$ films; (d)~(e) AFM phase images of BTR-Cl:$PC_{71}BM$, with $PC_{71}BM$ and w/o $PC_{71}BM$ films.

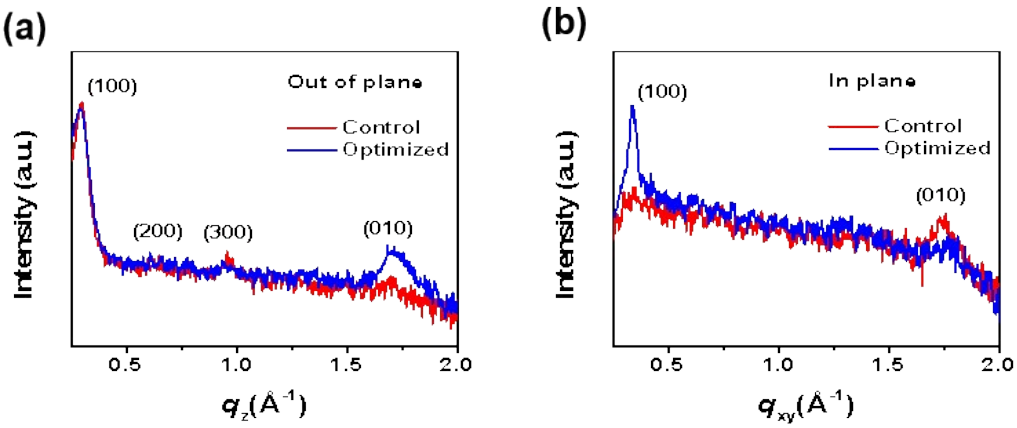

Figure S7. (a) and (b), In-plane (the dot lines) and out-of-plane (the solid lines) line-cut profiles of the corresponding two-dimensional GIWAXS data.

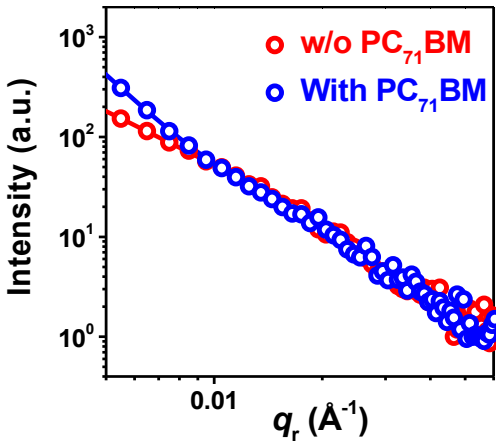

Figure S8. GISAXS intensity profiles (symbols) and the best fitting (solid lines) along the in-plane direction.

Table S5. Analysis data of the two-dimensional GIWAXS results in out-of-plane direction (OOP).

Blend film	Lattice plane	Peak location (A^{-1})	d-spacing (Å)	Coherence length (Å)
		q_z	q_z	q_z
Control	100	0.2913	21.55	125.99
	010	1.5999	3.73	27.05
Optimized	100	0.2914	21.55	123.51
	010	1.683	3.93	132.89

Table S6. Analysis data of the two-dimensional GIWAXS results.in in-plane direction (IP).

Blend film	Lattice plane	Peak location (A^{-1})	d-spacing (Å)	Coherence length (Å)
		q_{xy}	q_{xy}	q_{xy}
Control	100	0.337	18.64	193.20
	010	1.720	3.65	25.45
Optimized	100	0.337	18.64	152.80
	010	1.725	3.64	9.55

Table S7. Summary photovoltaic parameters of all-small-molecule organic solar cells with *PCE* over 10%.

Active Layer	*FF (%)*	*PCE (%)*	Active Layer	*FF (%)*	*PCE (%)*
BTR:NITI:$PC_{71}BM$	73.83	13.63[2]	BDTSTNTTR:$PC_{71}BM$	76.5	11.53[3]
DR3TSBDT:Y6:$PC_{71}BM$	67.27	12.84[4]	p-DTS($FBTTh_2$)$_2$:ZnP:$PC_{71}BM$	77.19	10.97[5]
BTR-OH:BTR:$PC_{71}BM$	74.2	10.41[6]	ZnP-TBO:6TIC	73.87	12.08[7]

SBDT-BDD:IDIC:$PC_{71}BM$	69.3	10.9[8]	SM:IDIC:$PC_{71}BM$	69.3	10.9[8]
DR3TBDTT:PC71BM:DR3TBDTT-S-E	76.9	10.38[9]	P2TBR:IDIC	70.1	11.5[10]
BSFTR:Y6	69.66	13.69[11]	DRCN5T:$PC_{71}BM$	68	10.08[12]
BDTTS-Cl-R:$PC_{71}BM$	75.3	10.78[13]	ZR1:Y6	68.44	14.34[14]
SM1:IDIC	73.55	10.11[15]	BTR-Cl:Y6	65.5	13.61[16]
BTID-2F:$PC_{71}BM$	76	11.3[17]	BETC-2F：Y6	72.35	13.34[19]
BTR:DIB-SQ:$PC_{71}BM$	73.8	10.3[18]	This Work	77.11	15.34

References:

1. L. Koster, E. Smits, V. Mihailetchi, P. Blom, *Physical Review B*, 2005, **72**, 085205.

2.Z. Zhou, S. Xu, J. Song, Y. Jin, Q. Yue, Y. Qian, F. Liu, F. Zhang and X. Zhu, *Nat Energy*, 2018, **3**, 952-959.

3.J. Wan, X. Xu, G. Zhang, Y. Li, K. Feng and Q. Peng, *Energ Environ Sci*, 2017, **10**, 1739-1745.

4.C. Xu, J. Wang, Q. An, X. Ma, Z. Hu, J. Gao, J. Zhang and F. Zhang, *Nano Energy*, 2019, **66**, 104119.

5.L. Nian, K. Gao, Y. Jiang, Q. Rong, X. Hu, D. Yuan, F. Liu, X. Peng, T. P. Russell and G. Zhou, *Adv Mater*, 2017, **29**, 1700616.

6.H. Tang, T. Xu, C. Yan, J. Gao, H. Yin, J. Lv, R. Singh, M. Kumar, T. Duan, Z. Kan, S. Lu and G. Li, *Adv Sci*, 2019, **6**, 1901613.

7.K. Gao, S. B. Jo, X. Shi, L. Nian, M. Zhang, Y. Kan, F. Lin, B. Kan, B. Xu, Q. Rong, L. Shui, F. Liu, X. Peng, G. Zhou, Y. Cao and A. K. Y. Jen, *Adv Mater*, 2019, **31**, 1807842.

8.Y. Huo, X. Gong, T. Lau, T. Xiao, C. Yan, X. Lu, G. Lu, X. Zhan and H. Zhang, *Chem Mater*, 2018, **30**, 8661-8668.

9.Y. Chang, Y. Chang, X. Zhu, X. Zhou, C. Yang, J. Zhang, K. Lu, X. Sun and Z. Wei, *Adv Energy Mater*, 2019, **9**, 1900190.

10.X. Li, Y. Wang, Q. Zhu, X. Guo, W. Ma, X. Ou, M. Zhang and Y. Li, *J Mater Chem a*, 2019, **7**, 3682-3690.

11.Q. Yue, H. Wu, Z. Zhou, M. Zhang, F. Liu and X. Zhu, *Adv Mater*, 2019, **31**, 1904283.

12.B. Kan, M. Li, Q. Zhang, F. Liu, X. Wan, Y. Wang, W. Ni, G. Long, X. Yang, H. Feng, Y. Zuo, M. Zhang, F. Huang, Y. Cao, T. P. Russell and Y. Chen, *J Am Chem Soc*, 2015, **137**, 3886-3893.

13.Z. Ji, X. Xu, G. Zhang, Y. Li and Q. Peng, *Nano Energy*, 2017, **40**, 214-223.

14.R. Zhou, Z. Jiang, C. Yang, J. Yu, J. Feng, M. A. Adil, D. Deng, W. Zou, J. Zhang, K. Lu, W. Ma, F. Gao and Z. Wei, *Nat Commun*, 2019, **10**, 5393.

15.B. Qiu, L. Xue, Y. Yang, H. Bin, Y. Zhang, C. Zhang, M. Xiao, K. Park, W. Morrison, Z. Zhang and Y. Li, *Chem Mater*, 2017, **29**, 7543-7553.

16.H. Chen, D. Hu, Q. Yang, J. Gao, J. Fu, K. Yang, H. He, S. Chen, Z. Kan, T. Duan, C. Yang, J. Ouyang, Z. Xiao, K. Sun and S. Lu, *Joule*, 2019, **3**, 3034-3047.

17.Y. Zhang, D. Deng, Z. Wang, Y. Wang, J. Zhang, J. Fang, Y. Yang, G. Lu, W. Ma and Z. Wei, *Adv Energy Mater*, 2017, **7**, 1701548.

18.M. Zhang, J. Wang, F. Zhang, Y. Mi, Q. An, W. Wang, X. Ma, J. Zhang and X. Liu, *Nano Energy*, 2017, **39**, 571-581.

19. J. F. Ge, L. C. Xie, R. X. Peng, B. Fanady, J. M. Huang, W. Song, T. T. Yan, W. X. Zhang, and Z. Y. Ge, *Angew. Chem. Int. Ed.*, 2020, **59**, 2808-2815.